First-principles study of diffusion and interactions of vacancies and hydrogen in hcp-titanium

Damien Connétable, Julitte Huez, Éric Andrieu and Claude Mijoule

CIRIMAT UMR 5085, CNRS-INP-UPS, École Nationale d'Ingénieurs en Arts Chimiques et Technologiques (ENSIACET) 4, Allée Émile Monso, BP 44362, F-31030 Toulouse Cedex 4, France

E-mail: damien.connetable@ensiacet.fr

doi:10.1088/0953-8984/23/40/405401

Abstract

We present a study of the stability of n-vacancies (V_n) and hydrogens in the hexagonal close-packed titanium system computed by means of first-principles calculations. In this work, performed by using the generalized gradient approximation of density functional theory, we focused on the formation energies and the processes of migration of these defects. In the first part, the calculated formation energy of the monovacancy presents a disagreement with experimental data, as already mentioned in the literature. The activation energy is underestimated by almost 20%. The stability of compact divacancies was then studied. We show that a divacancy is more stable than a monovacancy if their migration energies are of the same order of magnitude. We also predict that the migration process in the basal plane of the divacancy is controlled by an intermediate state corresponding to a body-centered triangle (BO site). The case of the trivacancies is finally considered from an energetic point of view. In the second part, the insertion of hydrogen and the processes of its migration are discussed. We obtain a satisfactory agreement with experimental measurements. The chemical nature of the interactions between hydrogen and titanium are discussed, and we show that the H-atom presents an anionic behavior in the metal. The trapping energy of hydrogen in a monovacancy as a function of the number of hydrogen atoms is finally presented.

(Some figures in this article are in colour only in the electronic version)

1. Introduction

Over a few decades, titanium alloys have evolved from being potentially important to being one of the most important structural materials, thanks to their specific properties which satisfy what is required from such a material, e.g. high specific strength and stiffness, good high temperature properties and corrosion behavior, high strength-to-weight ratio. Thus, titanium alloys are used in a wide field of applications, such as aerospace, power generation, and the chemical, medical, and sports industries, in which the thermal–chemical–mechanical environment is severe in terms of part durability. In some of these applications, titanium interacts with hydrogen, and while titanium's affinity for hydrogen is exploited for hydrogen storage or thermo-hydrogen processing, the interaction between Ti and H has to be controlled as it could also lead to a loss of mechanical properties. However, our understanding of the Ti–H system must be improved, including Ti–H reaction mechanisms, considering binding and the significance of the crystal structure in the reactions.

Hydrogen in metals has been extensively studied by means of first-principles calculations to understand the effects of hydrogen behavior, such as its solubility, long-range transport, and interaction with other lattice defects. Detailed simulations of hydrogen properties are available for hcp metals like Y [1], Zr [2], and Be [3]. Few descriptions have been proposed concerning multi-vacancy interactions and migration processes in hcp systems.

In this work we present a theoretical study of defects in the Ti system using first-principles calculations; *ab initio* calculations were performed to investigate the defect formation energies of vacancy defects in Ti–H system.

Table 1. Space group and Wyckoff positions of systems present in the phase diagram.

	Structure	Space group number	Wyckoff positions
α-Ti	Hexagonal close-packed (hcp)	194	2c
β-Ti	Body-centered cubic (bcc)	229	2a
ω-Ti	Hexagonal	191	1a, 2d
fcc-Ti	Face-centered cubic	225	4a

Particular attention is given to accounting for the chemical and migration processes of multi-vacancies and hydrogen, unlike in previous theoretical studies of the 'Ti–H' system [4].

The first part of this study focuses on a computational approach where the validity of Ti and H pseudo-potentials is discussed. The calculations are performed within the generalized gradient and pseudo-potential approaches and give results in good agreement with experimental data from the literature. In the second part, the formation, stability and migration of defects such as Ti-vacancies are studied in both hcp- and bcc-Ti. This leads to a discussion about the stability and the migration process of hydrogen in hcp-titanium. The migration processes of divacancies are also discussed, as is the issue of trivacancies from an energetic point of view. In the third part, hydrogen diffusion is investigated (energetic and migration aspects). The interaction between multi-hydrogens and monovacancies is also presented, and we conclude with the effect of insertion of hydrogen on the evolution of the lattice parameters.

2. Methodology and validity of pseudo-potentials

2.1. Computational approach

Our calculations were done within the density functional theory formalism (DFT) and the pseudo-potential approximation. They were performed by means of the Vienna *ab initio* simulation program (VASP) [5]. Projected augmented waves pseudo-potentials (PAW) [6] and the Perdew–Wang generalized gradient approximation (GGA) [7] of the exchange and correlation functional within its spin-polarized version were used. Plane-wave energy cut-off was fixed to 400 eV for all calculations, regardless of the size of the unit cell, and dense mesh grids equivalent to a $22 \times 22 \times 18$ **k**-mesh grid for a unit cell with two atoms (using a band folding approach) was used. The approach provides good convergence (1 meV/atom) with regard to experimental accuracy. Lattice relaxation, introduced by using a conjugate gradient algorithm, was taken into account; all ions and defects were allowed to relax.

2.2. Pseudo-potential approach

The crystalline structures, space group numbers and Wyckoff positions of different systems tested with the pseudo-potential Ti are listed in table 1.

The characteristics and properties of the structures were compared to those of the experimental measurements. In table 2, we report the formation energy of α-Ti, the cohesive energies for other structures, their lattice parameters, the elastic constants (for α-Ti only), the bulk modulus and the electron density of states.

The energy of the titanium atom was calculated, to obtain the cohesive energy. Spin polarization and the broken symmetry contributions were introduced. This improvement is not sufficient because the DFT approach is not efficient at describing the 'true' ground triplet state corresponding to the $3s^2 3p^6 4s^2 3d^2$ configuration. In fact, the latter must have a multi-referential character to be an eigenstate of the total kinetic moment $J = L + S$, while DFT only works with a single determinant. The mono-referential $3d^2 4s^2$ (^{3}F) triplet includes three eigenstates corresponding to $J = 2, 3, 4$ whose relative energies vary from 0 to 0.047 eV, respectively [8]. With these improvements, the calculated cohesive energy (E^{coh}) of α-Ti gives 4.74–4.79 eV, which is in agreement with experimental data, namely 4.85 eV (see table 2 [9]). α-Ti lattice parameters are well reproduced (1–2% discrepancy). Previous theoretical studies either used the local density functional LDA (FPLMTO [10, 11]), GGA functionals (FPLMTO [11, 12]) or the pseudo-potential approach [13–15] and FLAPW [16]. Theoretical results in the literature give similar values to those obtained in the present study. The elastic constants were also computed by means of a finite size deformations approach (see table 3). The agreement with experimental values is excellent.

The formation energies (E^{f}) of the other systems, were calculated by taking hcp-Ti as the reference state. We found, for example, that ω-Ti is slightly more stable than α-Ti as indicated by previous DFT calculations [22]. The fcc structure has a formation energy smaller than the β-Ti structure, independently of the choice of the functional (Perdew–Wang or Perdew–Burke–Ernzerhof).

The results, as a whole, on ground state properties validate the Ti pseudo-potential used in the following. The hydrogen pseudo-potential has been tested on the H_2 molecule. The inter-atomic distance (d(H–H) = 0.75 Å), the binding energy ($E_{\mathrm{f}} = -4.567$ eV), and the ground state frequency ($\omega = 129.9$ THz $= 537$ meV) were found to be in excellent agreement with experimental data [9].

3. Vacancies: formation and migration

n-Vacancies (denoted V_n) in hcp-Ti are discussed first. The study is restricted to monovacancies, divacancies and trivacancies, from an energetic and chemical point of view. For mono- and divacancies, we also looked at their diffusion mechanisms.

The super-cell size effects on the formation energies of V_n were considered in order to reduce interactions of

Table 2. Lattice parameters (in Å), bulk modulus (B_o, in GPa), cohesive energies (E^{coh}, in eV/atom) and formation energy (E^f, in eV/atom).

		a_0	c_0	c_0/a_0	B_o	E^{coh}
hcp (α)	Expt.	2.945[a]	4.544[a]	1.587[a]	110[a]	4.85[b]
	Theo.	2.932[c]	4.648[c]	1.585[c]	112[c]	4.74–4.79[c]
		2.990[a]	4.715[a]	1.577[a]	129[a]	
		2.99[d]	4.75[d]	1.59[d]		
		2.934[a]	4.638[a]	1.581[a]		
		2.930[e]	4.644[e]	1.585[e]	112[e]	
		a_0	c_0	c_0/a_0	B_o	E^f
bcc (β)	Expt.	3.264[d]			99 (116)[d]	71, 45[f]
	Theo.	3.241[c]			103[c]	109[c]
ω	Expt.	4.616[g]	2.806[g]	0.608[g]	105–138[g]	12, 13[h]
	Theo.	4.569[c]	2.828[c]	0.608[c]	111[c]	-7[c] (-10)[e]
fcc	Expt.	4.10[i]				
	Theo.	4.106[c]			108[c]	57[c]

[a] See [17] and cited references.
[b] Expt. from [9].
[c] Our GGA-VASP simulations.
[d] GGA SIESTA [18].
[e] GGA QE [22].
[f] Expt. extrapolated at $T = 0$ K [19].
[g] Expt. [20].
[h] Expt. extrapolated at $T = 0$ K [21].
[i] Expt. [23].

neighboring super-cell vacancies. The formation energy of V_n is then given by

$$H^f_{nv} = H^f(V_n) = E[(N-n) \times \text{Ti}, \Omega_1] - \frac{N-n}{N} E[N \times \text{Ti}, \Omega_0] \quad (1)$$

where $E[N \times \text{Ti}, \Omega]$ is the total energy of the super-cell with N atoms, and $E[(N-n) \times \text{Ti}, \Omega]$ the total energy with n-vacancies.

3.1. The monovacancy

3.1.1. Vacancy in hcp-Ti. Stability of the monovacancy. Results are listed in table 4 with theoretical and experimental data from the literature. The super-cell size effects are significantly strong. Large super-cells are thus needed to obtain converged values. The formation energy from our simulations (1.96 eV at 0 K) is in good agreement with that found by Raji *et al* [22]. It is smaller than previous theoretical first-principles studies: with a FPLMTO method, LeBacq found 2.14 eV [25] and Trinkle *et al* [26] 2.03 eV (GGA calculations). However, the experimental measurement is scattered and slightly different from *ab initio* values: the Doppler-broadened lineshapes of positron annihilation measurements give a formation energy of 1.27 eV [27].

A simple empirical rule has been established to correlate the formation energy of the monovacancy with the melting temperature (T_m) [25]: the enthalpies of formation of the defect are nearly proportional to the melting temperatures, as well as the enthalpies of self-diffusion and of vaporization, i.e. H^f_{1v} (eV) $\simeq 10^3\ T_m$ (in K). When $T_m \simeq 1948$ K for Ti, the value of $E^f_{1v} \simeq 1.95$ eV, i.e. close to our value.

Table 3. Elastic constants (in GPa) of hcp-Ti, compared with experiment, $C_{66} = (C_{11} - C_{12})/2$.

α-Ti	C_{11}	C_{33}	C_{44}	C_{12}	C_{66}	B_o
Expt.[a]	162.4	180.7	46.7	86.9	44.6	110.0
Theo.[b]	172.5	179.7	43.8	81.9	45.3	112.1

[a] Expt. from [24].
[b] GGA-VASP simulations.

The zero point energy (ZPE) contribution of the formation enthalpy of the monovacancy, H^{vib}_{1v}, is given by:

$$H^{vib}_{1v} = F_{vib}[(N-1) \times \text{Ti}] - \frac{N-1}{N} F_{vib}[N \times \text{Ti}] \quad (2)$$

where F_{vib} is the vibrational free energy, which has been computed in the harmonic approximation: $F_{vib} = \sum_{q,\nu} \hbar\omega_{q,\nu}/2$. We used a $3 \times 3 \times 2$ super-cell, and the summation on the full frequencies was calculated in $\mathbf{q} = \Gamma$. We found $H^{vib}_{1v} \simeq 3$ meV , of the same order of magnitude as expected for the monovacancy in fcc-Ni. To conclude, the ZPE leads to a slight increase in the stability of the monovacancy.

The disagreement between the experimental and theoretical values (around 0.61 eV) is somewhat unusual. The Doppler-broadened lineshapes of positron annihilation measurements were obtained at relatively low temperatures (500–900 K) [27], thus the thermal expansion lattice cannot explain such a difference. Semi-empirical potentials were adjusted on experimental data [31, 30], leading to difficulties in comparing them with our simulations. Moreover, in metal systems, the formation energy of a monovacancy is generally

Table 4. Formation and migration energies (in eV) of the vacancy with respect to the size of the super-cell. Two migration energies are given in the basal plane (noted $E^{\mathrm{m}}_{\parallel,1\mathrm{v}}$), and along $\langle c \rangle$ ($E^{\mathrm{m}}_{\perp,1\mathrm{v}}$).

	$2 \times 2 \times 2$	$3 \times 3 \times 2$	$4 \times 4 \times 3$	$5 \times 5 \times 4$
nb atom	16	32	96	200
$H^{\mathrm{f}}_{1\mathrm{v}}$ [a]	2.04/1.99	2.04/1.99	1.98/1.96	1.97/1.96
	$H^{\mathrm{m}}_{\parallel,1\mathrm{v}}$	$H^{\mathrm{m}}_{\perp,1\mathrm{v}}$	$H^{\mathrm{f}}_{1\mathrm{v}}$	$E^{a}_{\parallel/\perp,1\mathrm{v}}$
Theo.[a]	0.43	0.56	1.96	2.39/2.52
Other works	0.43[b]	0.57[b]	2.13[b]	2.63[b]
			2.14,[c] 1.97[d]	
			2.03,[e] 1.92[e]	
	0.61,[f] 0.58[g]	0.56,[f] 0.52[g]	1.50[f,g]	
Expt.			1.27[h]	3.14[i]

[a] Present work, GGA-VASP simulations, unrelaxed/relaxed shapes.
[b] GGA SIESTA [18].
[c] LDA FPLMTO [25].
[d] GGA QE [22].
[e] GGA-VASP [29].
[f] n-body potential [30].
[g] n-body potential [31].
[h] Expt. positron annihilation measurements [27].
[i] Expt. radio-tracer, and ion beam sputtering technique [33].

found to be smaller than the experimental value. Mattsson *et al* [28] proposed a procedure to evaluate the correction of the intrinsic surface error. Using their results on our system (number of electrons per atom, $N_{\mathrm{elec}} = 12$, electronic bulk density $\simeq 0.693$ Å^3, see [28]) at the first order of approximation, a value of around 0.50 eV (GGA functional) is found. The resulting formation energy of the monovacancy is equal to 2.5 eV.

Migration of the monovacancy. The atomic migration process of the monovacancy is controlled by its diffusion in and out of the basal planes, labeled $\parallel$ and $\perp$, respectively. The diffusion constants in hexagonal systems are thus computed from the following equations [35, 36]:

$$D_{\parallel,1\mathrm{v}} = D_{x,1\mathrm{v}} = D_{y,1\mathrm{v}} = \tfrac{1}{2}a^2(3\Gamma_{\parallel,1\mathrm{v}} + \Gamma_{\perp,1\mathrm{v}})C_{1\mathrm{v}} \quad (3)$$

for the component parallel to the basal plane, and

$$D_{\perp,1\mathrm{v}} = D_{z,1\mathrm{v}} = \tfrac{3}{4}c^2\Gamma_{\perp,1\mathrm{v}}C_{1\mathrm{v}} \quad (4)$$

for the perpendicular one. $C_{1\mathrm{v}}$ is the equilibrium monovacancy concentration at the temperature T, which may be approximated by

$$C_{1\mathrm{v}} = \exp\left[\frac{S^{\mathrm{f}}_{1\mathrm{v}}}{k_{\mathrm{B}}}\right]\exp\left[-\frac{H^{\mathrm{f}}_{1\mathrm{v}}}{k_{\mathrm{B}}T}\right] \simeq \exp\left[-\frac{H^{\mathrm{f}}_{1\mathrm{v}}}{k_{\mathrm{B}}T}\right] \quad (5)$$

where $H^{\mathrm{f}}_{1\mathrm{v}}$ is the free energy of vacancy formation. $\Gamma_{\parallel,1\mathrm{v}}$ and $\Gamma_{\perp,1\mathrm{v}}$ are the jump frequencies of the monovacancy in the basal and non-basal planes, respectively:

$$\Gamma_{\parallel/\perp,1\mathrm{v}} = \nu_{\parallel/\perp,1\mathrm{v}}\exp\left[-\frac{H^{\mathrm{m}}_{\parallel/\perp,1\mathrm{v}}}{k_{\mathrm{B}}T}\right] \quad (6)$$

where $H^{\mathrm{m}}_{\parallel/\perp,1\mathrm{v}}$ is the monovacancy migration free energy, and $\nu_{\parallel/\perp,1\mathrm{v}}$ are the atomic attempt frequencies. $\nu_{\parallel/\perp,1\mathrm{v}}$ is approximated from the ratio between the frequencies of the initial state (system with a monovacancy) (ω_i) and those of the transition state (ω^*_i) [37]:

$$\nu_{\parallel/\perp} = \frac{\prod_{i=1}^{3N}\omega_i}{\prod_{i=1}^{3N-1}\omega^*_i}. \quad (7)$$

The two possible transition states were studied with $4 \times 4 \times 3$ super-cells. The results of the migration energies are listed in table 4. Our values are in good agreement with those found by Vérité calculated with a similar approach [18]. From these migration energies and the formation energy, two activation energies of the monovacancy can be defined for parallel and perpendicular diffusion, equal to 2.41 and 2.54 eV respectively:

$$E^{a}_{\parallel/\perp,1\mathrm{v}} = H^{\mathrm{f}}_{1\mathrm{v}} + H^{\mathrm{m}}_{\parallel/\perp,1\mathrm{v}}. \quad (8)$$

Experimentally, Köpper *et al* determined by means of a ^{44}Ti radio-tracer and ion beam sputtering technique, the Arrhenius parameters for the Ti self-diffusion [33]. They found $Q_{\perp} = 3.14 \pm 0.02$ eV , and $D_{0,\perp} \simeq 1.4 \pm 0.4 \times 10^{-3}$ m^2 s^{-1}. From the activation energy, and by using our value of migration energy, we can deduce the formation energy of the monovacancy, 1.87 eV, which is significantly greater than those found by Hashimoto [27]. The comparison between theoretical and experimental values reveals some difficulties: the measured activation energy is associated with self-diffusion. The diffusion mechanism of a self-interstitial is more complex than a simple migration of a vacancy. It has been shown that in hcp systems dumbbell configurations should play a role in the self-diffusion mechanism (see for example [34]). Note that $D_{\parallel}/D_{\perp} < 1$ ($\simeq 0.23$–0.33 depending on the temperature) while $a_o/c_o < 1.633$.

To compute the atomic attempt frequencies, $\nu_{\parallel/\perp,1\mathrm{v}}$, we considered in a first approximation only frequencies of the

Table 5. Formation and migration energies of the vacancy in bcc-Ti for various sizes of the super-cell.

n atom	54 ($3 \times 3 \times 3$)	128 ($4 \times 4 \times 4$)	
H^{f}_{1v} [a]	2.03	2.03	
	H^{m}_{1v} (eV)	H^{f}_{1v} (eV)	H^{a}_{1v} (eV)
	—	2.20[b]	—
Expt.	0.72[c]	1.45,[c] 1.28,[d] 1.55[e]	2.17[c]

[a] Present work, GGA-VASP simulations, unrelaxed values.
[b] LDA FPLMTO [38].
[c] Expt. [39].
[d] Expt. [27].
[e] Expt. [32].

Ti-atom involved in the migration of the vacancy ($N = 1$, in equation (7)). We have thus calculated the three frequencies of the diffusing atom in its equilibrium lattice position (first nearest neighboring atom of the vacancy) and its frequencies in the configuration in which this atom is at the saddle point along the diffusion path. This approach allowed us to easily estimate ν_{1v}, the full frequency calculation being too time-consuming. The attempt frequencies were found to be equal to $\nu_{\parallel} = 31.1$ THz and $\nu_{\perp} = 37.3$ THz. From $E^{m}_{\parallel,\perp}$ and $\nu_{\parallel,\perp}$, we have calculated $D_{o,\parallel,\perp}$ by means of equations (3), (4) and (6). A linear regression of D_o with T (by means of the Arrhenius function) gives 2.36 and 2.54 eV for parallel and perpendicular activation energies, respectively.

As a partial conclusion with the monovacancy in hcp-Ti, we can underline the significant disagreement between experimental and *ab initio* values (about 0.6 eV). At this stage, as mentioned by Vérité [18], the disagreement is not clear: it could be due to anharmonic effects or impurities. The intrinsic surface error could also be at the origin of this difference.

3.1.2. Vacancy in bcc-Ti. We briefly discuss the monovacancy in β-Ti. The interest is to quantify, for this structure, the disagreement between theoretical and experimental values of the formation energies of the vacancy, and to compare it with the results obtained for hcp-Ti. Indeed, Neumann [39] and Hashimoto [27] have measured the formation and migration energies in bcc-Ti.

This system has a simple crystal structure, making calculations easy. In the case where the Ti-atoms are not relaxed, one finds a formation energy equal to 2.03 eV, compared to 2.20 eV from the theoretical literature [38, 25]. This value deduced from our approach is in good agreement with those of Le Bacq *et al* [25]. It is also greater than experimental measurements, obtained at high temperature, up to the phase transition temperature of 1150 K (from 1.28 to 1.55 eV see table 5).

However, when the atomic positions and the unit cell are relaxed, the formation energy became unphysical. The result depends strongly on the size of the super-cell, and atomic relaxations are too large. One can suspect that the monovacancy spontaneously induces a phase transition at 0 K, which can be related to vibrational properties of β-Ti (see, for example, [40]). β-Ti has soft modes along different crystallographic directions.

3.2. Divacancy in hcp-Ti

Divacancies are expected to contribute significantly to the diffusion process of interstitials and defects, as already shown in many metals (fcc-Ni [41], bcc-Fe [42] and fcc-Cu [43]) and insulator systems (Si–diamond) [44]. Also, they are well known to be at the origin of the nucleation step for loop clustering or cavity formation.

3.2.1. Stability of the divacancy. Various configurations were investigated to discuss the binding energy of the divacancy as a function of the distance between the monovacancies. There are two first nearest neighbor configurations: either in two adjacent planes (denoted AB) or in the same plane (AA); see figures 1(a) and (b), respectively. Since $a/c \neq \sqrt{3}/2$ in hcp-Ti, the distance between the vacancies is slightly different (2.87 and 2.93 Å, respectively). The other configurations (c)–(g) studied are also represented in figure 1.

The binding energy of the divacancy (E^{b}_{2v}) is defined from the formation energies of the mono- and divacancies as follows:

$$E^{b}_{2v} = H^{f}_{2v} - 2H^{f}_{1v} \tag{9}$$

where $H^{f}_{1v} = 1.96$ eV. With our convention, a negative binding energy corresponds to an attractive potential between the monovacancies. The results with $4 \times 4 \times 3$ super-cells (not reported here) are in agreement with those of Raji [22], or other empirical approaches [31, 30]. But larger super-cells were needed to reach convergent values. We report the results for $5 \times 5 \times 4$ super-cells in table 6.

Only compact divacancies (AA and AB) have negative binding energies (around -150 meV). Interactions were seen to decrease rapidly. Vacancy–vacancy should bind strongly and should be stabilized in comparison to isolated monovacancies. In other metals like fcc-nickel [41] and bcc-iron [42] similar results have been reported.

From a thermodynamic point of view, the (d) configuration can be considered as a limiting state in the formation of compact divacancies. The dissociation energy (out of plane) is equal to about 0.42 eV, while in-plane the dissociation energy falls to 0.21 eV (see figure 2).

3.2.2. Concentration of vacancies. Taking into account mono- and divacancies, the concentration of vacancies in titanium is given by

$$C_v = C_{1v} + 2\sum_i C_{2v,i} \tag{10}$$

where $C_{2v,i}$, the concentration of the divacancy labeled (i), is given by

$$C_{2v,i} = \frac{Z_i}{2} \exp\left[-\frac{H^{f}_{2v,i}}{k_B T}\right] \tag{11}$$

where the factor Z_i corresponds to the coordination number

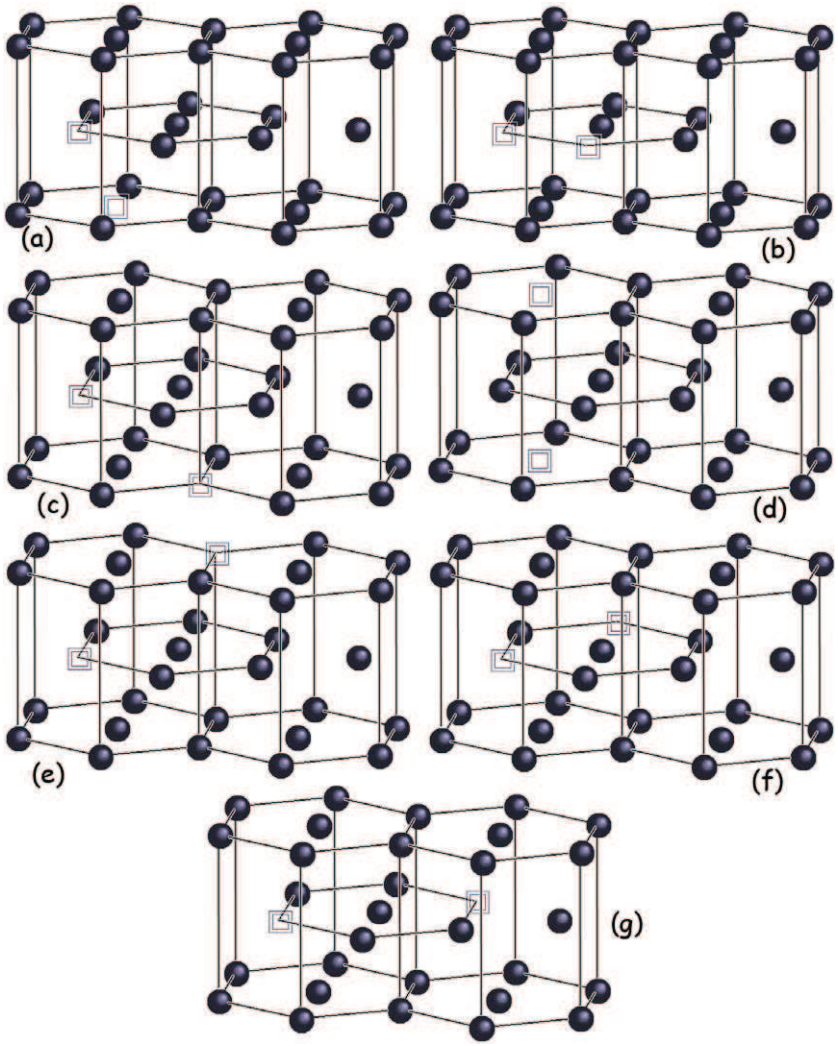

Figure 1. Schematic representation of different configurations of the divacancies studied. Letters correspond to the different configurations, used in the text, (a)–(g).

Table 6. Formation and binding energies (in eV), and distance between vacancies (d(V –V), in Å) in hcp-Ti.

Position	E^{f}_{2v} (eV)	E^{b}_{2v} (eV)	d(V –V) (Å)
(a) AB	3.77[a]	−0.15	2.87
	3.72[b], 3.92[c], 3.68[c],	−0.12[b]	
	2.78[d], 3.04[e]	−0.20[d], −0.14[e]	
(b) AA	3.79[a]	−0.13	2.93
	3.74[b], 2.79,[d] 3.03[e]	−0.10[b], 0.20[d], −0.16[e]	
(c)	4.02	0.10	4.11
(d)	4.20 (4.28[b])	0.28 (0.32[b])	4.65
(e)	3.97	0.05	5.05
(f)	3.97	+0.05	5.08
(g)	3.99	0.06	5.86

[a] VASP GGA, 5 × 5 × 4 super-cells.
[b] GGA QE [22].
[c] GGA-VASP [29].
[d] n-body potential [30].
[e] n-body potential [31].

of type i per lattice: $Z = 6$ for AB and AA. For the first order, we considered only AA and AB divacancies. At 1000 K, the concentration of vacancies is equal to $C_{1v} = 1.3 \times 10^{-8}$ and $C_{2v}/C_{1v} = 1.1 \times 10^{-6}$. At 300 K: $C_{1v} = 1.2 \times 10^{-32}$ and $C_{2v}/C_{1v} = 5.2 \times 10^{-27}$. Note that even at high temperatures the concentration of divacancies is low.

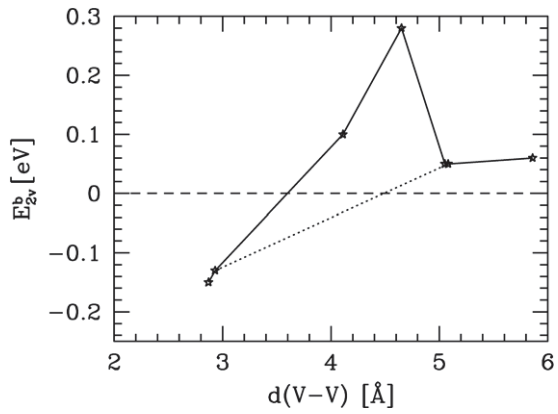

Figure 2. Binding energy versus distance between vacancies. Dotted lines: the binding energies of divacancies in a basal plane.

Table 7. Migration energies of the divacancies (E^m, in eV). Different cases are presented as a function of the initial states and of the path. AB–B, AA–B, AB–A and AA–A: XY–Z, X and Y are initial states, and Z is the final state of Y.

$E^m_{AB-B,2v}$	$E^m_{AA-B,2v}$	$E^m_{AB-A,2v}$	$E^m_{AA-A,2v,direct}$
0.40	0.25	0.28	0.51
			$E^m_{AA-A,2v,via\ BT}$
			0.36/0.08[a]

[a] AA divacancy or BT configuration as reference.

3.2.3. Migration of divacancies. The migration of divacancies AA and AB, i.e. cases (a) and (b), were investigated. Four different transition states were studied: AB–B, AA–B = AB–A and AA–A (XY–Z: X and Y are the initial states, and Z is the final state of Y (see figure 3)). The second configuration corresponds to two different diffusion processes, where the initial and the final configurations are switched (AA or AB). The results are summarized in table 7.

For the two first configurations, the migration energies are found to be nearly equal (0.40 and 0.43 eV; see table 7). These values are of the same order of magnitude as the migration value of the monovacancy.

In the third case—migration of the divacancy in the AA–A plane—a stable intermediate state was found. This configuration is represented in figures 5 and 4. The position of the Ti-atom corresponds to a body-centered triangle (labeled BO) formed by the three vacancies. The atom interacts with the top and bottom titanium of neighboring planes, and this configuration corresponds to a high symmetric position. The Ti-atom has six nearest neighbors. Its Bader net charge is found to be approximately the same as that of other titaniums. Such a configuration cannot be observed along the *c* axis.

To provide a better understanding of these states, we investigated other configurations: BT, O, T and S. For O, T and S, the states are energetically unfavored (see for example the case of O). In the case of the configuration BT, see table 8, the energy gap with BO is large (around 0.40 eV).

From an energy point of view, BO is slightly less stable than the AA divacancy, around 0.18/0.11 eV (5 × 5 × 4 super-cell simulation). Its binding energy is negative (−0.13 eV). This state could also be considered as an intermediate state during the migration of the AA divacancy in the plane.

Table 8. Comparison of the formation and binding energies of divacancies with an intermediate configuration: BO, BT and O.

Intermediate state	E^f (eV)	E^b (eV)
BO	3.98	0.06
BT	4.22	0.30
O	6.77	2.86

Table 9. Formation and binding energies (in eV) of a trivacancy in hcp-Ti.

Configuration	E^f_{3v}	E^t_{3v}	E^b_{3v}
(a) AAB	5.43	−0.37	−0.50
(b) AAA	5.22	−0.59	−0.71
(c)	5.71	−0.07	−0.20
(d)	5.74	−0.03	−0.15
(e)	5.88	+0.09	−0.03

Two new migration paths were also considered: a 'direct' migration between two Ti-sites, imposing the position of the Ti 'migrating' state, and an 'indirect' migration, using a path between BO and the AA divacancy. A direct migration requires 0.51 eV, while the 'indirect' path has a migration energy of 0.36 eV, only 0.08 eV up to the BO energy.

To conclude, divacancies are found to be stable defects. Their migration is easier than that of monovacancies.

3.3. Trivacancy clusters

We finally present the results of the formation energies of trivacancy clusters. Five V_3 configurations were investigated (see figure 6). We defined two binding energies from the formation energy of the trivacancy: the references states are one divacancy and one monovacancy, E^t_{3v}, which corresponds to the trapping of a monovacancy by a divacancy:

$$E^t_{3v} = E^f_{3v} - E^f_{2v} - E^f_{1v} \tag{12}$$

and E^b_{3v} the binding energy from three monovacancies:

$$E^b_{3v} = E^f_{3v} - 3E^f_{1v}. \tag{13}$$

A negative binding energy means that the trivacancy should be more stable than the reference(s). In table 9, the formation energy of both trivacancies and their associated binding energies are given. Note that two trivacancies are energetically favored in comparison to the di- and monovacancies. This result can be related that of multi-vacancies in fcc-Ni.

The most stable configuration is the most compact trivacancy (AAA). Furthermore the energetically favored defects are those located in the same plane. These results indicate that the formation of planar defects in hcp-Ti is favored.

4. Hydrogen in titanium

4.1. Insertion enthalpies

From a crystallographic point of view, hcp systems are partitioned in octahedral and tetrahedral volumes. In one unit

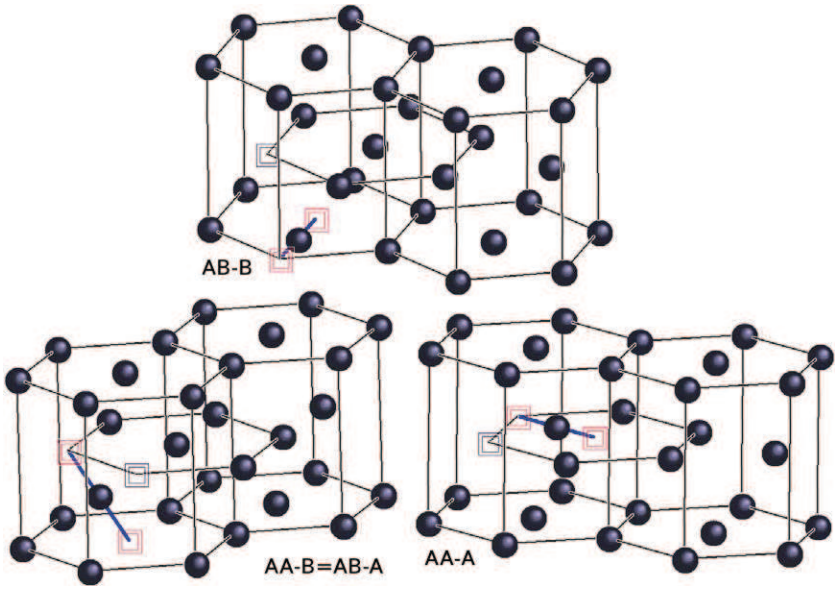

Figure 3. Schematic representations of saddle points in the migration processes of the divacancy in hcp-Ti. Vacancies are represented by squares and the pathways are symbolized by the bold lines connecting vacancies.

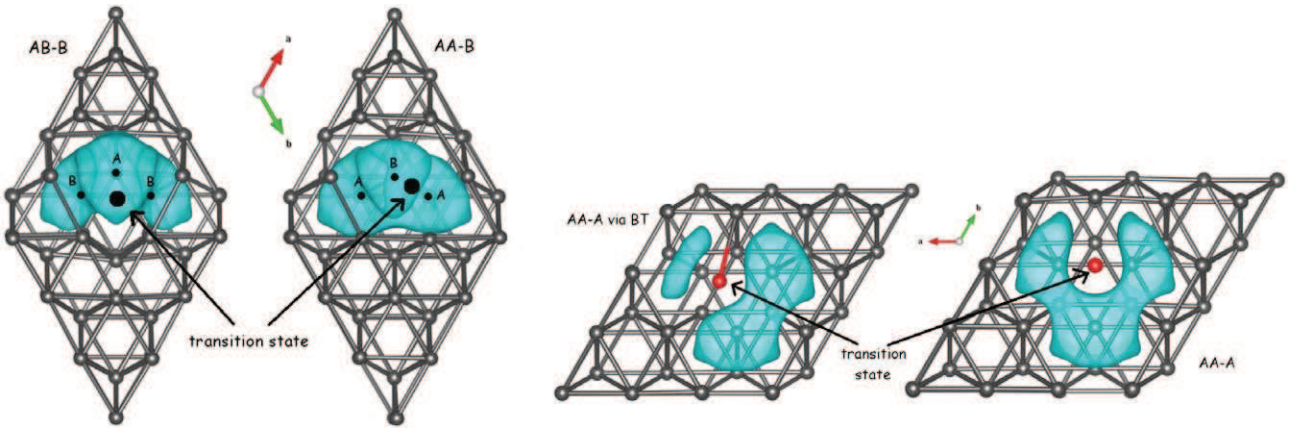

Figure 4. Low part of the electron density in the transition state AA–A (direct and via BT), AB–B, and AA–B.

cell, there are two equivalent octahedral sites (denoted O) and four equivalent tetrahedral sites (T). The tetrahedral site is located around 0.55 Å from the basal plane (see figure 8).

In the literature, the position of hydrogen remains unclear. Experimentally, Khoda *et al* have shown that, in hcp-Ti, hydrogen prefers the tetrahedral site (see [45] and references therein) as in hcp-Zr [2]. Hempelmann *et al* also found that hydrogen occupies tetrahedral sites [46]. All experimental results suggest that hydrogen prefers the tetrahedral site. The experimental insertion energy of hydrogen was measured to be equal to $\Delta H^o = -0.54$ and -0.62 eV for hcp- and bcc-Ti, respectively [47].

From the theoretical literature, the H-atom should prefer to be located in octahedral sites. Griessen [48] predicted, by means of a semi-empirical model, that octahedral sites should be 50 kJ/mol H ($\simeq 0.52$ eV) more stable than tetrahedral sites. Xu *et al* [4] also found that the octahedral sites are 76 meV more stable than the tetrahedral sites. And for Kang [49] (LDA and unrelaxed calculations), hydrogen in the octahedral sites is favored (3.43 eV binding energy) compared to the tetrahedral sites (3.10 eV).

The energy of solubility and insertion were provided, taking into account the dissociation of H_2, in the gas phase or not. The solubility C^{s} is given by

$$C^{\mathrm{s}} = C^{\mathrm{s}}_{\mathrm{H}} \exp\left[-\frac{E^{\mathrm{dis}}_{\mathrm{H}}}{k_{\mathrm{B}}T}\right] \tag{14}$$

with $C^{\mathrm{s}}_{\mathrm{H}} \propto \sqrt{P_{\mathrm{H}_2}}$ (P_{H_2} is the pressure in dihydrogen; see Fukai [47]), and where the energy of solubility, $E^{\mathrm{sol}}_{\mathrm{H}}$, is given by

$$E^{\mathrm{sol}}_{\mathrm{H}} = E[N \times \mathrm{Ti} + H] - E[N \times \mathrm{Ti}] - \frac{E[\mathrm{H}_2]}{2}. \tag{15}$$

$E(\mathrm{H}_2)$ is the total energy of the H_2 molecule in the gas phase. $E^{\mathrm{ins}}_{\mathrm{H}}$, the insertion energy, is defined as

$$E^{\mathrm{ins}}_{\mathrm{H}} = E[N \times \mathrm{Ti} + \mathrm{H}] - E[N \times \mathrm{Ti}] - E[\mathrm{H}]. \tag{16}$$

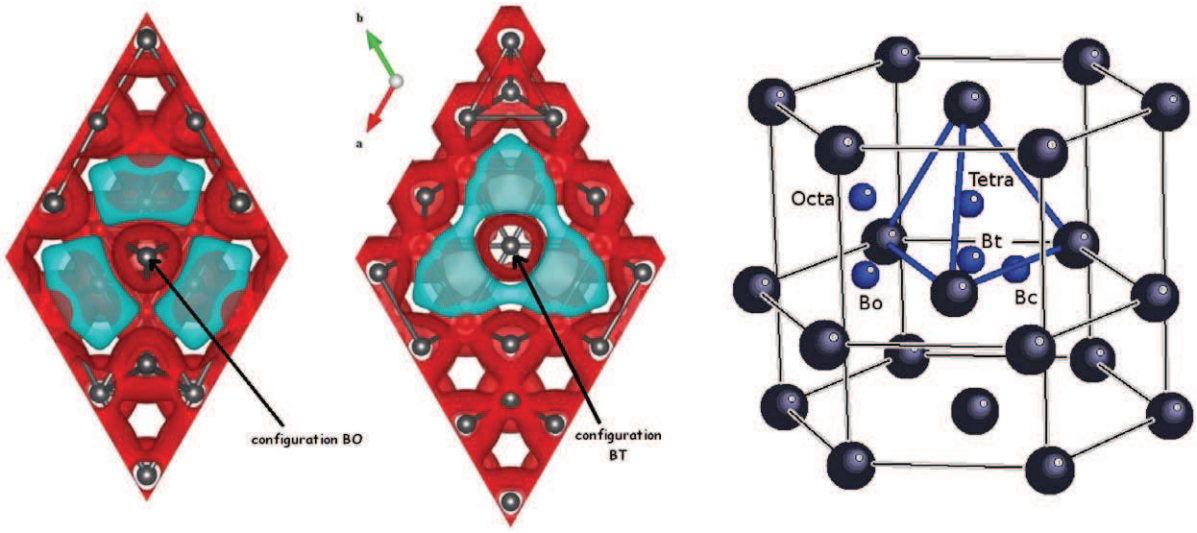

Figure 5. Electron density of two intermediate states (in blue, the 'low' part, and in red the highest): BO (left) and BT (center). Special positions in hcp systems (right).

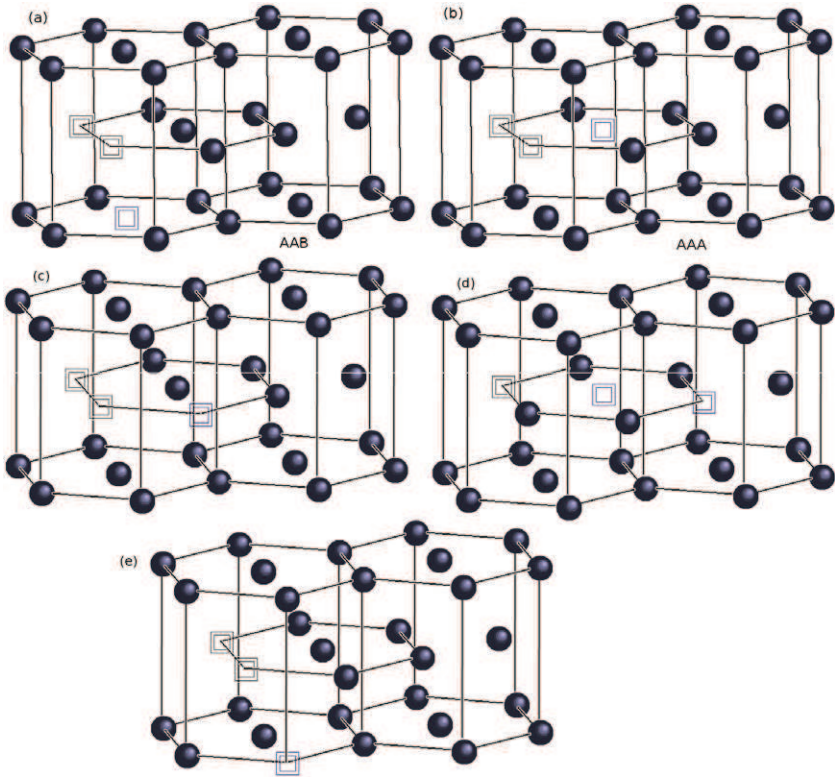

Figure 6. Schematic representations of the trivacancies studied.

In the case of substituted hydrogen, the energy ($E^{\mathrm{sol}}_{\mathrm{H,sub}}$) is then given by

$$E^{\mathrm{sol}}_{\mathrm{H,sub}} = E[(N-1)\times \mathrm{Ti} + \mathrm{H}] - E[N\times \mathrm{Ti}] - \frac{E[\mathrm{H_2}]}{2} - E^{\mathrm{f}}_{\mathrm{1v}}. \tag{17}$$

The results are listed in table 10. As in previous theoretical studies, the octahedral site was found to be energetically more stable than the tetrahedral one, from around 0.07 eV. The value of the solubility energy (−0.44 eV) is close to the experimental value (−0.54 eV).

The vibration frequencies of hydrogen have been computed in each site: in the case of the tetrahedral site they were 34 and 41 THz (doubly degenerate) (142 and 171 meV, respectively), and for octahedral insertion 26 (doubly degenerate) and 29 THz (107 and 121 meV respectively). The ZPE ($\sum \omega(\mathrm{H})/2$) is thus equal to 0.24 and 0.17 eV for the T and O sites, respectively. The fact

Table 10. Insertion, substitution (E_H^{dis} and E_H^{ins}) and zero point energies (E_v) at 0 K as a function of the size of the unit cell (in eV). Hydrogen is either in the substitution, the tetrahedral or the octahedral interstitial positions.

	$2 \times 2 \times 2$			$3 \times 3 \times 2$		$4 \times 4 \times 3$	
Super-cell	E_H^{sol}	E_H^{ins}	E_v	E_H^{dis}	E_H^{ins}	E_H^{dis}	E_H^{ins}
H_{sub}	8.18	5.90	<0[a]	8.27	5.99	8.23	5.95
H_T	−0.35	−2.63	0.24	−0.37	−2.65	−0.37	−2.65
H_O	−0.47	−2.75	0.17	−0.44	−2.72	−0.44	−2.72

[a] The configuration is unstable.

that the frequencies of the tetrahedral sites are greater than octahedral frequencies is consistent with the interactions. The lower of the frequencies of the octahedral sites in comparison to the tetrahedral sites is a consequence of weaker interactions between the host lattice and hydrogen in the octahedral site.

From this set of frequencies, we can calculate, in a first approximation, the ZPE correction for the insertion energy of hydrogen as a function of its position:

$$E_{vib}^{sol}[H_{O,T}] = F_{vib}[N \times Ti + H_{O,T}] - F_{vib}[N \times Ti] - \frac{F_{vib}[H_2]}{2} \simeq F_{vib}[H \text{ in } Ti] - \frac{F_{vib}[H_2]}{2}. \quad (18)$$

For H_2, the formation energy and vibrational frequency were also calculated ($E_f = -4.567$ eV, $\omega = 129.9$ THz $= 537$ meV , $F_{vib}[H_2] = 268$ meV). The energy was then corrected by 120 and 35 meV for T and O, respectively. These results do not modify the relative stability of the sites, the corrected solubility energies were found to be equal to −0.41 and −0.25 eV for O and T, respectively.

The theoretical frequencies of hydrogen at each site can be compared to experimental data. Hempelmann *et al* [46] measured the position of the optical phonon modes in the hydrogenated Ti phase by means of neutron scattering experiments. They found one peak of 150 meV at low temperature (about 25 °C), two peaks at a higher temperature (105.5 and 162 meV at 326 °C) for the H 'doped' phase, and only one large peak (108 meV) for deuterium doped hcp-Ti, regardless of the temperature.

The isotopic effects in the Einstein model, between the H and D elements, are due to the vibrational part of the energy. It is given approximately by $\omega(H)/\omega(D) \simeq \sqrt{2}$, which gives 106 from 150 meV for deuterium at low temperature, and 74 and 114 meV at higher T. Khoda-Bakhsh *et al* [45] also obtained the same results.

From our theoretical results we can reinterpret the experimental data. At low temperature, the main peak (at around 140 meV) is clearly associated with the tetrahedral site. The two other small peaks can be associated with the octahedral sites. At 715 °C, the three peaks (120, 150 and 170 meV) can be associated with the vibrations of the H-atoms in both sites. In conclusion, the experimental neutron scatterings indicate that, at low temperature, hydrogen (H or D) is preferentially located in tetrahedral sites, whereas at high temperature hydrogen is located in both sites.

We finally conclude with the case where hydrogens are considered in substitution. This configuration is energetically unfavored as suspected (−8.23 eV), and is an unstable state (imaginary frequencies).

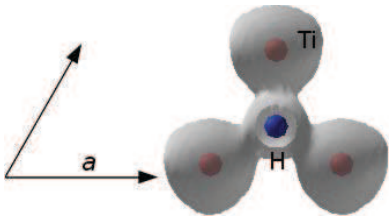

Figure 7. Representation of the lower part of the electron charge curve density of hydrogen in the tetrahedral position. Titanium atoms are in red and hydrogen in blue. hydrogen is above the basal plane represented by the three Ti.

4.2. Chemical interactions of H with Ti

The electron charge density for tetrahedral insertion is plotted in figure 7 to analyze the nature of interactions between H and Ti. The H-atom interacts with its four first Ti neighbors. A similar pattern is observed in the octahedral site, where the hydrogen interacts with its six nearest neighbors. The charge transfer between the diffusing H-atom and the surrounding Ti has also been examined, using Bader's analysis [50]. According to the total electron count related to hydrogen in hcp-Ti, the charge on hydrogen is close to 1.8 and 1.7 for octahedral and tetrahedral sites, respectively. Hydrogen becomes partially anionic ($+0.7e$) when inserted in the bulk, as already observed in α-Fe [42] and fcc-Ni [51].

4.3. Migration process of hydrogen

To understand the atomic migration process of hydrogen in hcp-Ti, five transition states were considered. They correspond to the saddle points in the high symmetric configurations. They are represented in figure 8: path (1) corresponds to a transition along $\langle c \rangle$ between two tetrahedral sites (out of plane); path (2) corresponds to a transition between two neighboring tetrahedral sites in the basal plane (along the $\frac{1}{12}[4\bar{4}03]$ direction); path (3) corresponds to a transition state between two neighboring octahedral sites in the basal plane; path (4) is located between two octahedral sites along $\langle c \rangle$ axis; and the configuration (5) corresponds to a transition between T and O. The migration energies are dependent of the initial position (either O or T).

The easiest transition arises between two tetrahedral sites (see table 11), a migration path neglected by Han [55]. These results can be directly compared to those of hcp-Zr systems [2]. The two migration paths (T–T along the $\frac{1}{12}[4\bar{4}03]$

Table 11. Migration and zero point energies of each path for hcp-Ti and hcp-Zr [52]. 'nsp' indicates that the configuration does not correspond to a saddle point.

Path	T–T	T–T	O–O	O–O	T–O	O–T
			Titanium			
	$\langle c \rangle$	$\frac{1}{12}[4\bar{4}03]$	$\langle a \rangle$	$\langle c \rangle$		
E^{m} (eV)	0.12	0.66	0.79	0.65	0.39	0.46
Other Works[a]	—	—	0.62	0.69	0.33	0.51
Expt.			0.54,[b] 0.64[c]			
ω_ν (meV)	206, 209	nsp	nsp	208, 210	195, 186	
ω_ν (THz)	50, 51	—	—	50, 51	47, 45	
			Zirconium			
E^{m} (eV)	0.12	0.74	0.70	0.41	0.36	0.41
ω_ν (THz)	43, 43	nsp	nsp	47, 47	43, 46	

[a] GGA [55].
[b] Expt. [56].
[c] Expt. [57].
[d] Theo. [52].

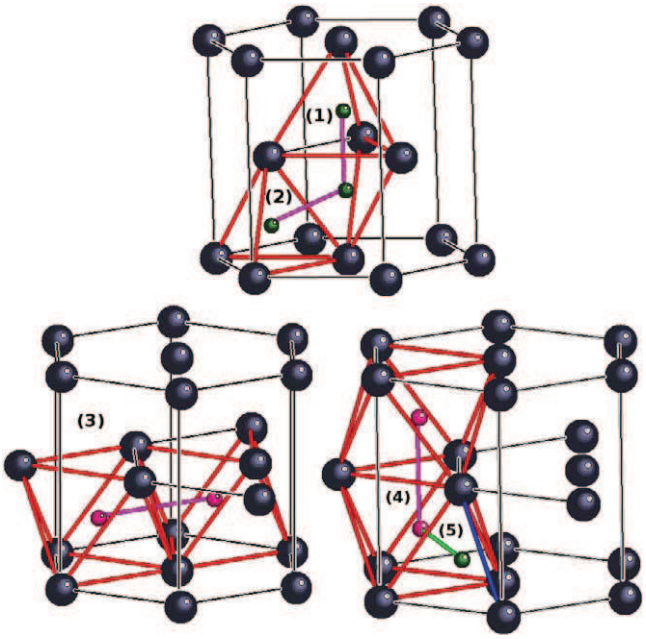

Figure 8. Schematic representation of the five transition paths in the hcp system between octahedral and tetrahedral sites. Hydrogen in an octahedral site is in rose, and hydrogen in a tetrahedral site is green.

direction and O–O $\langle a \rangle$) do not correspond to 'true' transition states. They are characterized by two imaginary frequencies, unlike a saddle point.

The jump frequency for hydrogen is given by

$$\nu = \nu_o \exp\left[-\frac{E^{\mathrm{m}}}{k_{\mathrm{B}}T}\right] \tag{19}$$

where ν_o is, to the first order, approximated by [37]:

$$\nu_o = \frac{\prod_{i=1}^{3} \omega_i(\mathrm{H})}{\prod_{i=1}^{2} \omega_i^*(\mathrm{H})} \tag{20}$$

Table 12. Migration energies and jump frequency of hydrogen for the different migration processes.

Migration path	E^{m} (eV)	ν_o (THz)
T → T	0.12	22
O → O	0.65	8
T → O	0.39	27
O → T	0.46	9

where ω_i are frequencies in the initial position and ω_i^* the frequencies in the transition state. The frequencies of the H-atom in tetrahedral sites were found to be equal to about 41, 41 and 34 THz, and in octahedral sites about 26, 26 and 29 THz. The diffusion parameters (E_{m} and ν_o) are listed in table 12.

From these results, the migration energies in each main direction (parallel and perpendicular to the basal plane, labeled $\parallel$, $\perp$, respectively) can be computed. The isotopic effects are deduced from these results by a factor of 0.707 of all frequencies in the case of deuterium diffusion. The formation and migration energies are still the same.

4.4. Effect on lattice parameters of hydrogen

In order to complete this study, the insertion of hydrogen into hcp-Ti tetrahedral and octahedral sites and the effect of the concentration of hydrogen on the lattice parameters is discussed. Margolin [53, 54] has shown that hydrogen insertion induces an anisotropic expansion of the unit cell. They found $\lambda_a = 0.02$ and $\lambda_c = 0.008$, where λ_a and λ_c correspond to the hydrogen expansion in and out of the basal plane, respectively: $\lambda_a = \frac{1}{a}\frac{\mathrm{d}a}{\mathrm{d}x_{\mathrm{H}}}$ and $\lambda_c = \frac{1}{c}\frac{\mathrm{d}c}{\mathrm{d}x_{\mathrm{H}}}$. Unlike zirconium, for hcp-Ti the dilatation of the lattice parameter in the $\langle a \rangle$ direction is greater than in the $\langle c \rangle$ direction.

From our simulations, we estimated λ_a and λ_c. We found in the case of hydrogen in octahedral sites that $\lambda_a \simeq 0.039 \pm 0.010$ and $\lambda_c \simeq 0.019 \pm 0.005$ (calculated with $2 \times 2 \times 2$ and $3 \times 3 \times 3$ super-cells). In the case of hydrogen in tetrahedral

Table 13. Formation and binding energies of H_2 (in eV) in two neighboring interstitial sites.

Configuration	E^f (eV)	$E^b(H_2)$ (eV)	d(H–H) (Å)
T–T	−0.30	+0.56	1.65
T–O	−0.73	+0.14	1.99
O–O	−0.87	−0.00	2.92

sites, the trend is the same as in octahedral sites but the numerical value is too small to be usable, which makes the comparison of experiment and theory difficult. These results show a good order of magnitude and the trend of experimental data.

4.5. H–H interactions

Interactions between hydrogen atoms in two different neighboring interstitial sites were studied. Three configurations were investigated: one hydrogen in T and the other in the O, two hydrogens in tetrahedral sites (T–T) and two hydrogens in octahedral sites (O–O). The binding energy of H–H is then calculated from

$$E^b(H_2) = E^f(H_2, Ti) - 2E^f(H_1, Ti) \quad (21)$$

where $E^f(H_1, Ti)$ corresponds to the insertion energy of hydrogen in an octahedral site. H–H interactions were found to be repulsive (see table 13), which can be explained partially by the anionic character of hydrogen in titanium. One can also note the rapid decrease of the interactions between hydrogens.

4.6. Vacancy–hydrogen complexes (VH_n clusters)

Vacancies in metals are suggested to be an efficient trap for hydrogen atoms. We also studied the decoration of the monovacancy by hydrogen. Many symmetrical cases of VH_n ($n \in [1, 5]$) configurations were considered, and fully relaxed.

4.6.1. VH_1. As shown previously, the substituted configuration is unstable, which leads to the restoration of the monovacancy. We also investigated three different configurations: hydrogen is moved out of the plane (along the c direction, labeled 'out'), or hydrogen is moved in the plane either toward (a) one or (b) two Ti-atoms (see figure 9).

In the first case, if the initial shift is small, hydrogen almost falls into the vacancy. The potential surface of hydrogen along z is flat, which explains why the relaxed distance between the H-atom and vacancy (d(V–H) $\simeq$ 0.04 Å) is small. By symmetry, the H-atom cannot move in the plane. However, when the initial position is large enough, hydrogen migrates to the tetrahedral site, which is the nearest stable configuration.

When hydrogen is pushed toward one Ti-atom (*Bc* position), it prefers to move toward the Ti–Ti bond (see figure 9 (a), the BT final position). Energetically, the last configuration, which corresponds to the BT position, is the most stable configuration. The Ti-atoms above and below stabilize the hydrogen. The atomic distances are d(V–H) = 1.14 Å, and d(Ti–H) = 2.01 Å, and the Bader charge is found to be equal to 1.5 for the BO position. The distance between the vacancy and the H-atom is greater in BT: d(V–H) = 1.47 Å, d(Ti–H) = 1.87 Å in the plane and d(Ti–H) = 2.27 Å out of the plane, the Bader charge is equal to 1.6. As we will see in the following, the second configuration is always energetically favored. Its net charge is increased, and hydrogen forms bonds with Ti-atoms.

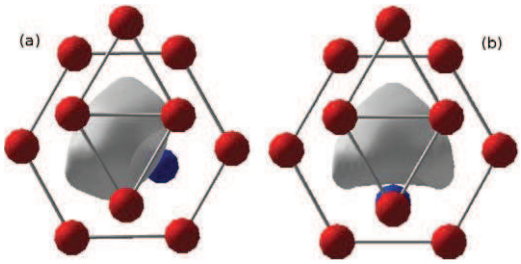

Figure 9. Representation of the electron charge density of hydrogen in the substitutional position: hydrogen toward Ti–Ti bonds (a) without and (b) with Ti-atoms directly in the plane above, i.e. sites BO and BT, respectively.

4.6.2. VH_2. For VH_2, we considered five configurations to place the hydrogens around the vacancy. In three configurations, they are located in the plane (see figure 10(c), (e) and (f)), and in the last one, H-atoms are above and below on both sides of the plane (a and b). As already mentioned for VH_1, the most stable configurations are those in which at least one hydrogen is located below a titanium (BT). We found that this most stable position corresponds to the (f) configuration, where the two hydrogens are located on both sides of Ti-atoms.

4.6.3. VH_{3-5}. From the two previous configurations, different symmetric configurations for VH_n defects where $n \in [3, 5, 6, 8]$ were studied. For VH_3, we have considered only one case: the hydrogens are in the same plane and in the BT position (see figure 11), while for VH_5, two cases were considered: two atoms in addition to VH_3 are on both sides of the plane and the last three hydrogens are located in the plane.

4.7. Discussion

Let us now consider the trapping of hydrogen by a vacancy. We define the trapping energy as the capacity for an existing VH_{n-1} defect to trap a H-atom present in an octahedral site by

$$E^{trap}(H_n) = E[H_n + V_{1,Ti}] - E[H_{n-1} + V_{1,Ti}] - E^{ins}[H, octa] \quad (22)$$

where E^{ins}[H, octa] is the insertion energy of hydrogen in an octahedral site, calculated below. We also define the insertion energy of n H-atoms as

$$E^{ins}(H_n) = E[H_n + V_{1,Ti}] - E[V_{1,Ti}] - nE_0(H). \quad (23)$$

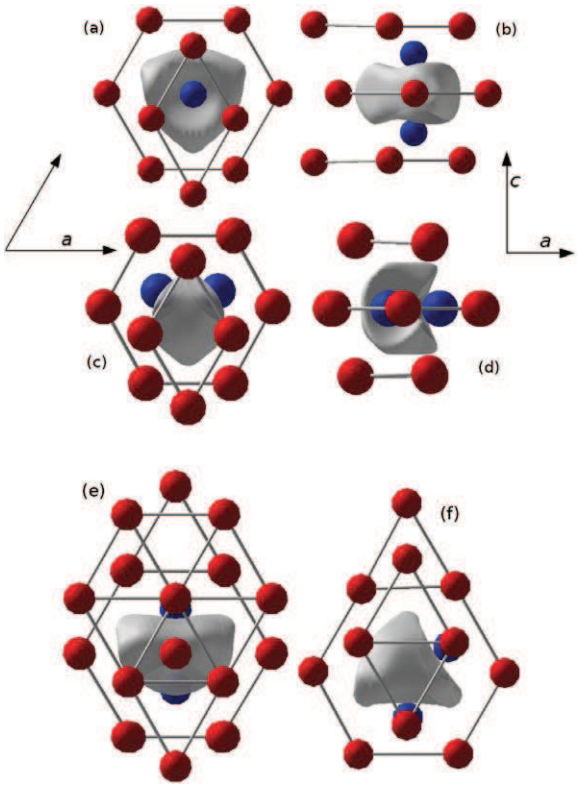

Figure 10. Representation of the electron charge density of VH_2: (a) and (b) H-atoms are out of the plane; in (c) and (d) they are in the BO–BO configurations in the basal plane (bottom); (e) and (f) correspond to the BT–BO and BT–BT.

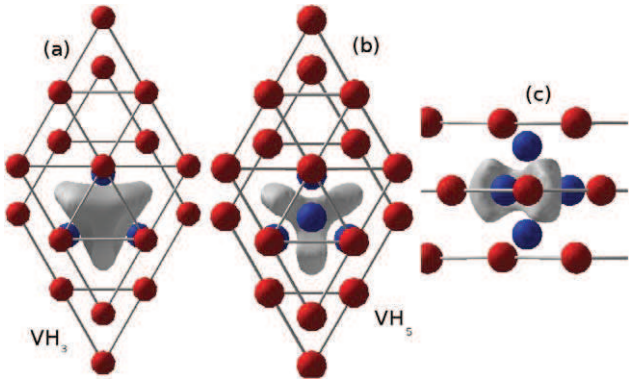

Figure 11. Representation of the electron charge density of VH_3 (a) and VH_5 ((b) and (c)).

Our results are listed in table 14. The first remark is that insertion is always energetically favorable. As in many systems (Al, Fe, Pb) in Ti, vacancies can trap hydrogen. In the case of hcp-Ti, one vacancy can trap up to three hydrogens.

5. Conclusion

We report a complete study of the interaction and migration processes of multi-vacancies and hydrogen in hcp-titanium. In the case of a monovacancy, in spite of an agreement with previous theoretical studies, our formation energy is found to be greater than that recorded experimentally. In contrast, the activation energy of the monovacancy is underestimated by about 20%. The present study was unable to explain such a disagreement. Our results on the divacancies show that the compact configurations are more energetically stable than two isolated monovacancies. However, the low concentration seems to indicate that divacancies could not be preponderant defects. A new configuration (BO) of the divacancy is shown to occur. Thanks to this new state, migration is easier for the divacancies than for the monovacancy. Finally, we show that the compact trivacancies are much more stable than bi- and monovacancies. These results should be considered with respect to the discrepancy noted between theoretical and experimental values of the formation of monovacancies. Experimental data should be revisited to take divacancies into account.

In the second part, we presented the migration of hydrogen in titanium. The hydrogen formation and migration energies were calculated, to enable their diffusion coefficients to be determined. At 0 K, hydrogen is predicted to prefer the octahedral site, in contradiction to experimental fact. Experimental vibrations of the H-atom are, however, well reproduced in our simulations. The migration process indicates that the H-atoms should diffuse more easily through tetrahedral sites.

We finally considered H-atoms trapped in a vacancy. The maximum number of hydrogens trapped in a monovacancy was found to be three.

Table 14. Trapping energies (in eV) of hydrogen(s) in V H_n ($n \in [1, 8]$), and atomic distance between hydrogens (in Å) for simple cases.

	E^{ins} (eV)	E^{trap} (eV)	d(H–H) (Å)
VH_1 ('out')	−1.81	−0.21	—
(a)	−2.32	−0.72	—
(b)	−2.95	−1.35	—
VH_2 (a, b)	−5.64	0.03	2.67
(c,d)	−4.71	0.95	2.02
(e)	−5.37	0.30	2.43
(f)	−5.96	−0.29	2.45
VH_3	−8.96	−0.29	2.42
VH_5	−14.37	0.03	2.11/2.56/3.02

Acknowledgment

This work was granted access to the HPC resources of CALMIP (CICT Toulouse, France) under the allocation 2009/2010-p0749 and 2010-p0842.

References

[1] Wang Y and Chou M Y 1994 *Phys. Rev.* B **49** 13357
[2] Domain C, Besson R and Legris A 2002 *Acta Mater.* **50** 3513
[3] Ganchenkova M G, Borodin V A and Nieminen R M 2009 *Phys. Rev.* B **79** 134101
[4] Xu Q and Van der Ven A 2007 *Phys. Rev.* B **76** 064207
[5] Kresse G and Hafner J 1993 *Phys. Rev.* B **47** 558
Kresse G and Hafner J 1994 *Phys. Rev.* B **49** 14251
Kresse G and Furthmüller J 1996 *Phys. Rev.* B **54** 11169
Kresse G and Furthmüller J 1996 *Comput. Mater. Sci.* **6** 15

[6] Kresse G and Joubert D 1999 *Phys. Rev.* B **59** 1758
[7] Wang Y and Perdew J P 1991 *Phys. Rev.* B **44** 13 298
[8] http://physics.nist.gov/PhysRefData/ASD/index.html
[9] Kittel C 1996 *Introduction to Solid State Physics* (New York: Wiley)
[10] Ahuja R, Wills J M, Johansson B and Eriksson O 1993 *Phys. Rev.* B **48** 16269
[11] Jomard G, Magaud L and Pasturel A 1998 *Phil. Mag.* **77** 67
[12] Kutepov A L and Kutepova S G 2003 *Phys. Rev.* B **67** 132102
[13] Trinkle D R, Hennig R G, Srinivasan S G, Hatch D M, Jones M D, Stokes H T, Albers R C and Wilkins J W 2003 *Phys. Rev. Lett.* **91** 025701
[14] Hennig R, Tinkle D, Bouchet J, Srinivasan S, Albers R and Wilkins J 2005 *Nature Mater.* **4** 129
[15] Trinkle D R, Hatch D M, Stokes H T, Hennig R G and Albers R C 2005 *Phys. Rev.* B **72** 014105
[16] Greeff C W, Trinkle D R and Albers R C 2001 *J. Appl. Phys.* **90** 2221
[17] Trinité V 2005 *Thesis* Ecole Polytechnique
[18] Vérité G, Willaime F and Fu C C 2007 *Solid State Phenom.* **129** 75
[19] Spreadborough J and Christian J 1959 *Proc. Phys. Soc.* **74** 5 609
[20] Chase M, Davies C, Downey J, Frurip D, McDonald R and Syverud A 1985 *J. Phys. Chem. Ref. Data* **14** (Suppl. 1) 1856
[21] Jamieson J 1963 *Science* **140** 72
[22] Raji A T, Scandolo S, Mazzarello R, Nsengiyumva S, Hrting M and Britton D T 2009 *Phil. Mag.* **89** 1629
[23] Vullum P E, Pitt M, Walmsley J, Hauback B and Holmestad R 2009 *Appl. Phys.* A **94** 787
[24] Fisher E and Renken C 1964 *Phys. Rev.* A **135** 482
[25] Le Bacq O, Willaime F and Pasturel A 1999 *Phys. Rev.* B **59** 8508
[26] Trinkle D R, Jones M D, Hennig R G, Rudin S P, Albers R C and Wilkins J W 2006 *Phys. Rev.* B **73** 094123
[27] Hashimoto E, Morita Y and Kino T 1984 *J. Phys. F: Met. Phys.* **14** 879
[28] Mattsson T R and Mattsson A E 2002 *Phys. Rev.* B **66** 214110
[29] Hennig R G, Lenosky T J, Trinkle D R, Rudin S P and Wilkins J W 2008 *Phys. Rev.* B **78** 054121
[30] Hu W, Zhang B, Huang B, Gao F and Bacon D J 2001 *J. Phys.: Condens. Matter* **13** 1193
[31] Dai Y, Li J H and Liu B X 2009 *J. Phys.: Condens. Matter* **21** 385402
[32] Kraftmakher Y 1998 *Phys. Rep.* **299** 79
[33] Köppers M, Derdau D, Friesel M and Herzig C 1997 *Def. Diffusion Forum* **143–147** 43
[34] Willaime F 2003 *J. Nucl. Mater.* **323** 205
[35] Philibert J 1995 *Atom Movements: Diffusion and Mass Transport in Solids* (*Monographies de Physique*) (Les Ulis: EDP Sciences)
[36] Monti A M and Savino E J 1981 *Phys. Rev.* B **23** 6494
[37] Vineyard G H 1957 *J. Phys. Chem. Solids* **3** 121
[38] Willaime F, Saitta A, Nastar M and Le Bacq O 2000 *Int. J. Quantum Chem.* **77** 927
[39] Neumann G, Tlle V and Tuijn C 2001 *Physica* B **296** 334
[40] Hu C E, Zeng Z Y, Zhang L, Chen X R, Cai L C and Alf D 2010 *J. Appl. Phys.* **107** 093509
[41] Megchiche E H, Mijoule C and Amarouche M 2010 *J. Phys.: Condens. Matter* **23** 48562
[42] Kandaskalov D, Mijoule C and Connétable D 2011 in preparation
[43] Andersson D A and Simak S I 2004 *Phys. Rev.* B **70** 115108
[44] Caliste D and Pochet P 2006 *Phys. Rev. Lett.* **97** 135901
[45] Khoda-Bakhsh R and Ross D K 1982 *J. Phys. F: Met. Phys.* **12** 15
[46] Hempelmann R, Richter D and Stritzker B 1982 *J. Phys. F: Met. Phys.* **12** 79
[47] Fukai Y 2005 *The Metal-Hydrogen System* (*Springer Series in Materials Science*) 2nd edn (Berlin: Springer)
[48] Griessen R 1988 *Phys. Rev.* B **38** 3690
[49] Kang M-H and Wilkins J W 1990 *Phys. Rev.* B **41** 10182
[50] Henkelman G, Arnaldsson A and Jónsson H 2006 *Comput. Mater. Sci.* **36** 354
[51] Connétable D and Mijoule C 2011 unpublished results
[52] Domain C 2001 *Thesis* University Lille
[53] Margolin H and Portisch H 1968 *Trans. Metall. Soc. AIME* **242** 1901
[54] Feaugas X and Conforto E 2009 *PlastOx 2007* p 161
[55] Han X L, Wang Q, Sun D L, Sun T and Guo Q 2009 *Int. J. Hydrogen Energy* **34** 3983
[56] Wasilewski R J and Kehl G L 1954 *Metallurgia* **50** 225
[57] Papazoiglou T P and Hepworth M T 1968 *Trans. Metall. Soc. AIME* **242** 682